Solar-Light-Driven N-TiO_2-SiO_2 Photocatalytic Activity on the Simultaneous Removal of Bisphenol-A and *Escherichia coli*

Minh Vien Le[1,2*], Trung Tan Tran[1,2], Anh Hoang Hoang[1,2], Hien Thao Nguyen[1,2], Vu Truong-Son Le[3], Van Hoang Luan[1,2], and Manh Thang Ngo[1,2]

[1]*Faculty of Chemical Engineering, Ho Chi Minh City University of Technology (HCMUT), 268 Ly Thuong Kiet Street, District 10, Ho Chi Minh City 700000, Vietnam*

[2]*Vietnam National University Ho Chi Minh City, Linh Trung Ward, Thu Duc, Ho Chi Minh City 700000, Vietnam*

[3]*University of Science and Education, University of Danang, 459 Ton Duc Thang Street, Da Nang City 550000, Vietnam*

* ***Corresponding author:***

email: lmvien@hcmut.edu.vn

Received: August 22, 2024
Accepted: January 2, 2025

DOI: 10.22146/ijc.99313

Abstract: *N-doped TiO_2-SiO_2 nanocomposites were synthesized using a facile sol-gel method and characterized through various techniques. Their photocatalytic performance was assessed by degrading BPA (10 mg L^{-1}) and inactivating* Escherichia coli *(~10^9 CFU mL^{-1}) under single and dual contaminant conditions using a 26 W solar light simulator. Among the synthesized materials, the N-TiO_2-SiO_2 nanocomposite with a 10% N:Ti molar ratio (TS5N10) demonstrated the highest photocatalytic activity, achieving 83.9% BPA degradation and complete* E. coli *disinfection in single contaminant systems after 4 h of irradiation. Notably, TS5N10 exhibited robust performance even in dual-contaminant scenarios involving BPA and* E. coli. *Mechanistic investigations identified photo-generated holes as the dominant reactive species. The superior performance of TS5N10 was attributed to its nanostructure, high specific surface area, strong light absorption, and reduced photoinduced electron-hole recombination. These results highlight the potential of TS5N10 for practical water treatment applications.*

Keywords: *bisphenol A degradation;* Escherichia coli *inactivation; photocatalysis; simultaneous removal; TiO_2*

■ INTRODUCTION

Over the past few decades, the scarcity of clean and safe water sources has been increasing and worsening, directly endangering the environment, ecosystem, and human health. The effluents from human activities often contain hazardous substances, including organic pollutants and pathogenic microorganisms, which pose serious risks to aquatic ecosystem and public health. Addressing this critical environmental challenge requires sustainable industrial practices and concerted efforts to preserve water quality [1-2]. Among organic contaminants, aromatic compounds are of particular concern due to their widespread use in industries such as textiles, pesticide, petrochemical, plastic, and rubber manufacturing. These compounds are non-biodegradable, highly toxic [3], and resistant to removal due to the stability conferred by their benzene ring structures and substituents [4]. Consequently, they readily enter the environment, leading to bioaccumulation and public health risks.

Bisphenol-A (BPA), for example, is widely employed in the production of pesticides, flame retardants, polycarbonate, and epoxy resins and is recognized as an endocrine disruptor [5]. Upon entering the human body through the aquatic system, BPA can bind to estrogen receptors in cellular nuclei, disrupting cellular activities and hormonal balance. In addition to chemical contaminants, pathogenic microorganisms such as *Escherichia coli*, often found in municipal wastewater, contribute to waterborne diseases [6]. These pathogens can lead to severe and sometimes fatal illnesses, including tuberculosis, blood inflammation,

pneumonia, and hemorrhage [7]. Alarmingly, both bacteria pathogens and aromatic compounds are frequently detected in industrial and domestic wastewater [8]. This dual presence underscores the urgent need for an effective strategy to simultaneously treat these harmful agents before wastewater is discharged into the environment. Developing innovative and efficient treatment methods is imperative to mitigate health hazards and ensure sustainable water management.

Titanium dioxide (TiO_2) is widely regarded as one of the most effective photocatalysts for addressing water pollutants issues. It enables the non-selective degradation of organic contaminants [9] and exhibits exceptional performance in the inactivation of microorganisms [10-12]. However, the practical application of TiO_2 is hindered by several limitations, including its wide bandgap energy (E_g ~3.2 eV), low specific surface area, and rapid recombination of photogenerated charge carriers, which reduce its efficiency, particularly under solar light irradiation [13-14]. To overcome these drawbacks, various strategies have been proposed to enhance the photocatalytic activity of TiO_2, including heteroatom doping [15], incorporation of high surface area material [14,16], and heterojunction construction [17]. Among these approaches, the integration of nitrogen doping and SiO_2 addition within the TiO_2 structure (N-doped TiO_2-SiO_2) has emerged as a promising strategy for developing photocatalysts capable of operating efficiently under solar light. Nitrogen atoms can easily substitute oxygen atoms in the TiO_2 lattice due to their comparable atomic size, polarizability, and electronegativity [13,18]. This substitution results in the formation of new energy levels of N_{2p} and oxygen vacancies between the valence and conduction band of TiO_2, leading to a narrowed bandgap energy [19]. Furthermore, N-doping has been shown to suppress the recombination rate of photogenerated charge carriers by capturing photogenerated electrons, thereby extending their lifetime [20]. As a result, N-doped TiO_2 can absorb light more effectively as well as generate more reactive species for the photocatalytic process, thereby enhancing the overall photocatalytic performance. Specifically, the TiO_2 sample containing 5 wt.% urea demonstrates the highest rhodamine B photodegradation efficiency, which can be attributed to the synergistic effects of N-doping and the coexistence of anatase and brookite phases. However, when the urea concentration exceeds 15 wt.%, the photocatalytic efficiency declines due to the formation of ketenimine impurities in the amorphous phase. These impurities act as recombination sites, thereby reducing photocatalytic activity [21]. Conversely, a previous study found that a TiO_2-SiO_2 composite with 30 mol% nitrogen doping achieved the optimal nitrogen content. Therefore, optimal nitrogen concentration requires further elaboration and investigation [22].

On the other hand, incorporating SiO_2 into the TiO_2 matrix effectively inhibits the growth of TiO_2 grains, resulting in an increased specific surface area of TiO_2. This expansion provides more active sites for photocatalytic reactions, thereby enhancing the material's capacity for pollutant remediation [23]. Consequently, N-doped TiO_2-SiO_2 emerges as a highly promising candidate for strengthening and improving photocatalytic activity, making it a robust material for environmental applications. However, while many studies have explored its photocatalytic performance for either pollutant degradation or bacterial inactivation [24-27], little attention has been given to its effectiveness in simultaneously treating complex systems containing both organic pollutants and bacteria [28-29].

This study aims to modify TiO_2 to enhance its photocatalytic activity for the simultaneous degradation of aromatic compounds and disinfection of bacteria. To achieve this, N-doped TiO_2-SiO_2 photocatalysts with varying amounts of N-doping were prepared using a simple sol-gel method. Optimal synthetic conditions for N-doped TiO_2-SiO_2 were determined by evaluating the influence of N-dopant content on the material's structural, optical, and photocatalytic properties. In this study, BPA and *E. coli* were selected as typical representatives of aromatic compounds and bacteria strains, respectively, to evaluate the photocatalytic and antibacterial activity of the synthesized materials under artificial solar irradiation. Moreover, the contribution of reactive species to the oxidation processes was clarified through radical scavenging experiments to determine

the primary active species driving the reactions. To comprehensively assess the performance of the N-doped TiO_2-SiO_2 catalyst, photocatalytic treatments targeting individual BPA and *E. coli*, as well as their mixture, were conducted under artificial sunlight. These experiments confirmed the catalyst's effectiveness in simultaneously degrading organic pollutants and disinfecting bacterial contaminants, demonstrating its potential for advanced environmental remediation applications.

■ EXPERIMENTAL SECTION

Materials

All chemicals and reagents were used as received without further purification. Titanium *n*-butoxide (TNB, 99%) was obtained from Acros Organics. Tetraethyl orthosilicate (TEOS, 99%), acetylacetone (AcAc, 99%), nitric acid (HNO_3, 65%), sodium chloride (99%), polypeptone, bacto yeast extract, and agar were all supplied by Merck (Germany). Polyethylene glycol (PEG, MW = 20000) and BPA (99%) were purchased from Sigma-Aldrich (Germany). Absolute ethanol (EtOH, 99.5%) was acquired from Cemaco (Vietnam). Deionized water (DI) was used in all experiments.

Instrumentation

X-ray diffraction (XRD) was performed for characterizing the crystal phases of the prepared samples by using a D2 Phaser-Bruker diffractometer with $\lambda_{Cu\ K\alpha}$ of 0.15418 nm, a scanning rate of 0.02 °/s, a scanning range from 20 to 80°. Furthermore, the surface morphology of N-doped TiO_2-SiO_2 was achieved using a field-emission scanning electron microscope (FE-SEM, Hitachi S-4800). The N_2 absorption-desorption isotherms were measured using the Quantachrome NOVA 1000e instrument. The specific surface areas and pore size distributions were calculated using Brunauer-Emmett-Teller (BET) and Barrett–Joyner–Halenda (BJH) methods. UV-vis diffuse reflectance spectra (DRS) were obtained to study light absorption and bandgap of photocatalysts by using a solid UV-vis JASCO V-550 spectrophotometer in a range from 250 to 800 nm. The bandgap energies (E_g) of samples were determined by using Tauc's equation as described in our previous publication [30]. The photoluminescence (PL) spectrum was recorded by a HORIBA Jobin YVON iHR 320 instrument with a wavelength range of 350 to 620 nm.

Procedure

Fabrication of N-doped TiO_2-SiO_2 catalyst

As described in our previous work, the N-doped TiO_2-SiO_2 photocatalysts were fabricated by sol-gel strategy [26]. In a typical process, a mixture was prepared by adding 5 mL EtOH, urea (with N molar percentages over Ti of 5, 10, and 15%), 1.2 mL of AcAc, and 0.5 mL of concentrated HNO_3 sequentially to a beaker containing 4.00 g of TNB. The mixture was stirred at 80 °C for 60 min to obtain solution A. Simultaneously, solution B was prepared by stirring the mixture of TEOS (Ti: Si molar ratio of 95:5), 0.20 g PEG, EtOH (5 mL), DI (2.4 mL), and concentrated HNO_3 (0.5 mL) at room temperature for 30 min. Afterward, solution B was gradually added dropwise to solution A while maintaining continuous stirring to achieve a homogeneous solution. This solution was then aged at room temperature for 45 h before being dried at 120 °C for 180 min. Eventually, the resulting powder was calcined at 500 °C for 120 min to obtain the final product. The N-doped TiO_2-SiO_2 samples were denoted as TS5N5, TS5N10, and TS5N15, according to the N molar percentages of 5, 10, and 15%, respectively. For comparison, the pristine TiO_2 and TiO_2-SiO_2 (TS5) were also prepared following the same procedure without adding TEOS and/or urea precursors.

Photocatalytic degradation of BPA

The photocatalytic activities of the synthesized materials were evaluated by the degradation of 10 mg L^{-1} BPA solution under simulated solar light, as described in our previous publication [26]. Typically, 0.200 g of catalyst was dispersed into a photo-reactor containing 200 mL of BPA solution and stirred in the dark for 60 min to reach adsorption/desorption equilibrium. The suspension was then exposed to simulated solar light from 26 W Exo Terra Lamp while continuously stirred for 4 h at a temperature of 30 ± 5 °C. At predetermined intervals, approximately 5 mL of the suspension was withdrawn using a syringe and passed through a 0.45 μm

nylon syringe filter to separate the catalyst from the aliquot. The residual BPA concentration was determined using a Hitachi U2910 UV-vis spectrometer at a wavelength (λ) of 225 nm, as described in our previous report [26].

In addition, scavenging experiments were conducted to investigate the contribution of reactive species to BPA photodegradation. For this purpose, 1.0 mM ethylenediaminetetraacetic acid disodium (EDTA-2Na), 1.0 mM isopropyl alcohol (IPA), and 1.0 mM para-benzoquinone (p-BQ) were employed as scavengers for trapping holes (h^+), hydroxyl radicals (•OH), and superoxide ($•O^{2-}$) radicals, respectively.

Photocatalytic inactivation of E. coli

Antibacterial activity was evaluated on *E. coli* K12 W3110 strain cultured on Luria Bertani (LB) broth following the method described by Tamer et al. [31]. The culture was incubated with a shaking rate of 150 rpm at room temperature for 18 h before being used. The resulting *E. coli* culture with the density of ~10^9 CFU mL^{-1} was cleaned to remove residual LB media and then diluted in sterilized NaCl 0.8% (w/w) solution to acquire an *E. coli* suspension with bacteria concentration of about 10^6 CFU mL^{-1}. For the antibacterial test, a 200 mL *E. coli* suspension was placed inside the photo-reactor. Subsequently, a 0.20 g photocatalyst was added, and the lamp was immediately turned on to start the testing. A control experiment was conducted simultaneously in the dark using another 200 mL of *E. coli* suspension without the photocatalyst. Samples from the suspensions were taken every 30 min during experimental time, then diluted in the NaCl 0.8% (w/w) solution with 10-fold serial dilution factors (*D*). Afterward, 100 µL of diluted samples were spread on Petri plates containing the autoclaved LB agar medium with agar content of 1.5% (w/w) to incubate at 37 °C for 24 h. *E. coli* density in the suspension (*C*) was calculated based on the number of colonies on a plate (*N*) according to Eq. (1).

$$C(\text{CFU mL}^{-1}) = N \times D \times 10 \quad (1)$$

Simultaneous treatment of BPA and E. coli

To investigate the simultaneous degradation of BPA and inactivation of *E. coli*, a solution containing 10 mg L^{-1} BPA and 10^6 CFU mL^{-1} was prepared in saline solution since the hypoosmotic stress in DI water can kill *E. coli* cells [29]. The best synthesized material was selected to test its photocatalytic activity in this dual-contaminant medium. The procedures for measuring BPA concentration and *E. coli* cell density over time were conducted in the same way described in previous sections.

■ RESULTS AND DISCUSSION

Characterization of Catalysts

The crystal phases of all prepared samples were analyzed using XRD technique, and the results are illustrated in Fig. 1. The XRD pattern of pristine TiO_2 exhibits characteristic peaks at 2θ = 25.3°, 37.8°, 47.9°, 53.8°, 55.1°, and 62.7°, corresponding to the of (101), (004), (200), (105), (211), and (213) crystal planes, respectively, of anatase TiO_2 structure (JCPDS 21-1272). In the TS5 sample, the absence of a SiO_2 crystal phase and the reduction in peak intensity indicate that SiO_2 is present in an amorphous phase and contributes to reducing the crystallite size. Similar findings were reported by Ren et al. [32], who observed that a 5% molar ratio of SiO_2 in TiO_2/SiO_2 composites inhibited the development of TiO_2 crystals. The reduction in crystallite size of composite oxides of TS5 is attributed to the formation of Si–O networks, which obstruct the growth of anatase crystallites [33]. In addition, the variation in crystal size may result from the agglomerates of primary particles, influencing the overall crystallization process [34]. All TS5 samples doped with nitrogen atoms show a pure anatase phase without any detectable extra peak, indicating the substitution of nitrogen into the TS5 structure does not alter the original crystal phase of TS5. On the other hand, the peak shift at the (101) plane of N-doped samples suggests that nitrogen atoms are incorporated into substitutional or interstitial positions within the TiO_2 crystal lattice [35]. This incorporation induces lattice distortion in the TiO_2 structure. Consequently, the crystallite size and unit cell parameters of the N-doped samples exhibit significant changes, as detailed in Table 1. These peak shifts, along with the alterations in crystalline structure and unit cell distortion, confirm the

incorporation of nitrogen atoms into the TiO_2-SiO_2 matrix.

The surface morphology of the TS5N10 sample was examined by FE-SEM images at various magnifications. Fig. 2 reveals that the TS5N10 sample consists of spherical particles with an uneven size distribution, ranging from 0.5 to 8 μm. The surface area and the pore structure of the TS5N10 sample were examined using N_2 adsorption-desorption isotherm recorded at 77 K. As shown in Fig. 3, the TS5N10 sample exhibited a type IV isotherm with an H3 hysteresis loop, indicating the presence of mesoporous structure. The specific surface area of TS5N10 was calculated to be 191.1 $m^2 g^{-1}$, which is comparable to that of the TS5 sample and approximately 5.7 times larger than that of pristine TiO_2, as reported in our previous work [27]. The BJH pore size distribution

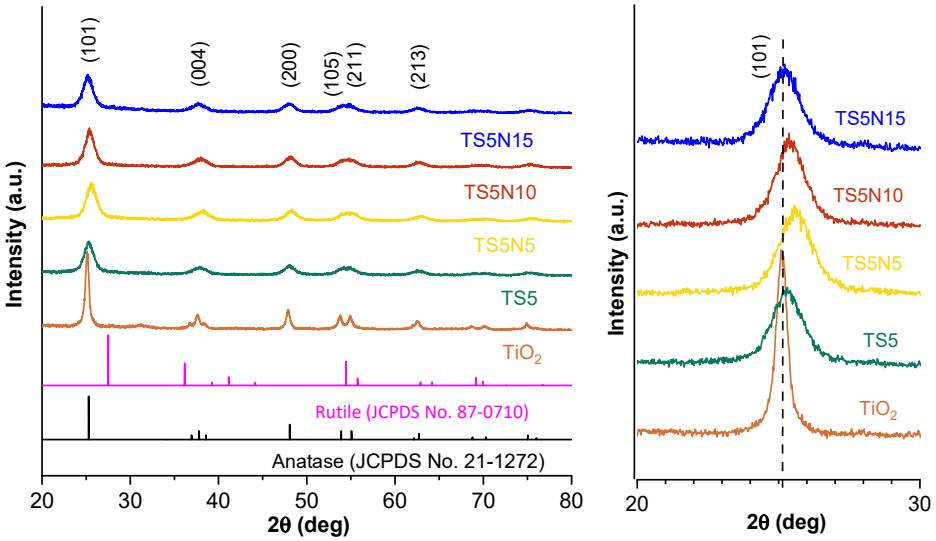

Fig 1. XRD patterns of pristine TiO_2, TS5 and N-doped TS5 composite with various nitrogen contents

Table 1. Crystallite size and unit cell parameter of samples

Sample	Crystallite size (nm)	$D_{(101)}$ (nm)	Unit cell	
			a=b (Å)	c (Å)
TiO_2	17.2	17.9	3.7964	9.5580
TS5	5.0	6.5	3.7854	9.5094
TS5N5	4.8	6.4	3.7629	9.3067
TS5N10	5.9	7.4	3.7394	9.4218
TS5N15	5.6	5.4	3.7877	9.5540

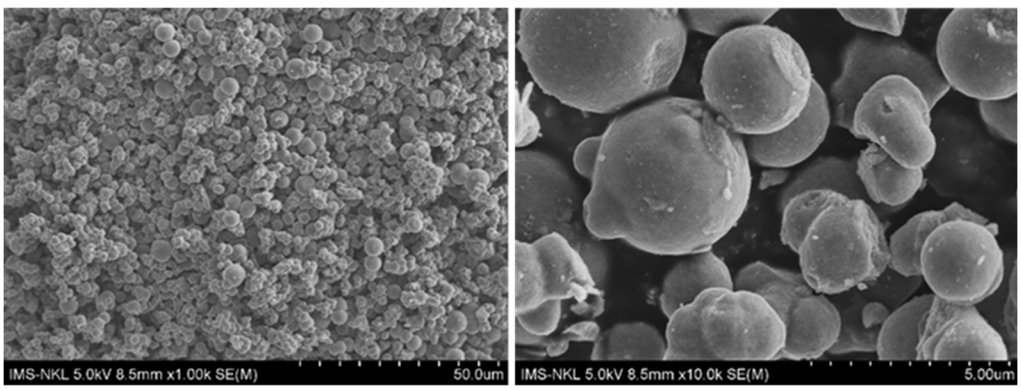

Fig 2. SEM images of TS5N10 at different magnifications

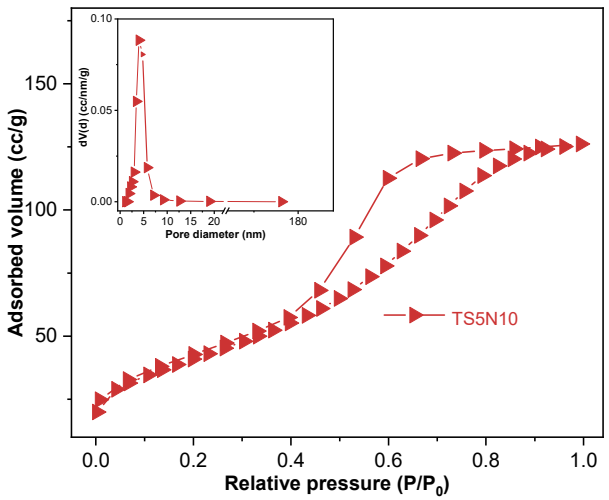

Fig 3. Nitrogen adsorption-desorption isotherm and (inset) BJH pore size distribution of N-doped TiO_2/SiO_2 composite (TS5N10)

analysis further confirms that TS5N10 predominantly consists of mesopores, with an average pore diameter of 4.01 nm. This mesoporous structure, coupled with the high specific surface area, provides a large number of available active sites accessible to contaminants. These features enhance the material's photocatalytic performance by facilitating the generation of reactive species, thereby improving its efficiency in pollutant degradation and bacterial disinfection.

Fig. 4 reveals the optical properties and band gap energies of prepared samples, as determined by UV-vis DRS. As shown in Fig. 4(a), the TS5N10 sample exhibits the strongest light absorption across the wavelength range of 250–800 nm, making it highly suitable for photocatalytic applications under solar light irradiation. The bandgap energies, calculated using Tauc's method (Fig. 4(b)), reveal a decrease from 2.95 eV for the TS5 sample to 2.82 eV for the TS5N10, in accordance with TS5 and TS5N10, respectively. This reduction in bandgap energy is attributed to the formation of intermediate energy levels or the overlapping of N_{2p} and O_{2p} orbitals states above the valence band. Additionally, the oxygen vacancies introduced by nitrogen doping serve as color centers, enhancing light harvesting and further improving the material's photocatalytic performance [36].

PL analysis was employed to elucidate the charge transfer behaviors of the catalysts. As depicted in Fig. 5, the pristine TiO_2 displays the highest PL intensity, indicating rapid recombination of photogenerated e^--h^+ pairs. In contrast, the TS5 exhibits the lower emission peak around 510 nm, attributed to the suppression of e^-/h^+ recombination under visible light. Significantly, the PL intensity of the TS5N10 sample is considerably lower than that of TS5, indicating improved charge carrier separation and a slower recombination rate. This reduced PL intensity in TS5N10 can be ascribed to the transfer of photogenerated electrons from the valence

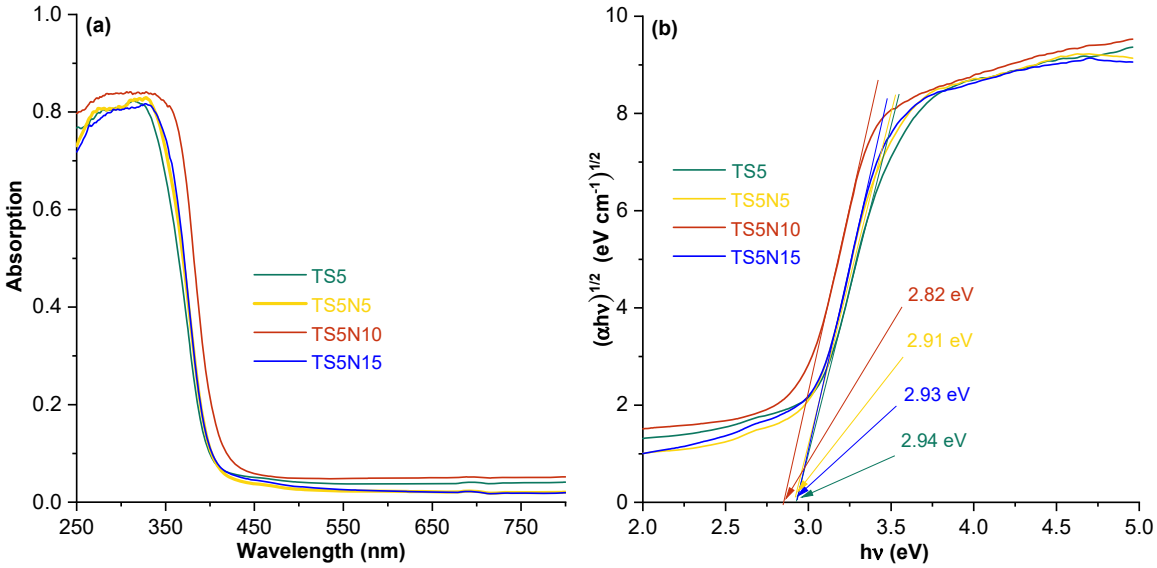

Fig 4. (a) UV-vis DRS spectra and (b) band gap energies of N-doped TS5 samples

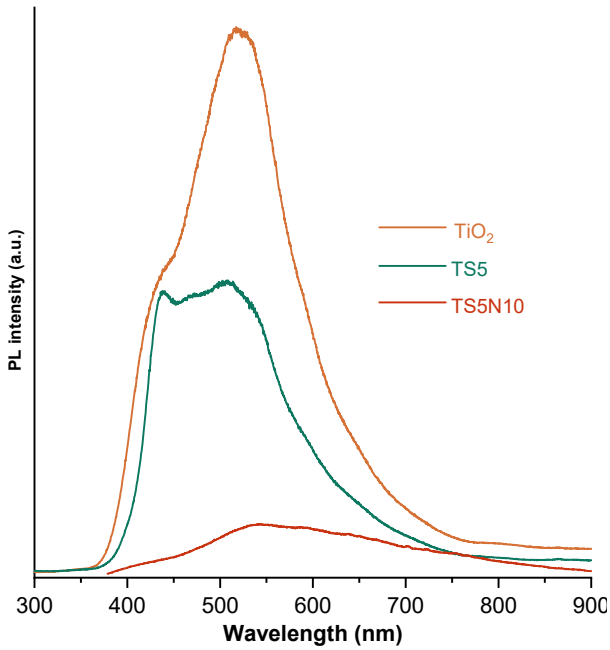

Fig 5. PL spectra of the pure TiO_2, TS5, and TS5N10 samples

band to energy levels above the conduction band induced by nitrogen doping [37] or the role of surface states (surface nitrogen species) and nitrogen states near the valence band as hole reservoirs [38]. The prolonged lifetimes of photogenerated electrons and holes in TS5N10 are expected to facilitate the formation of more reactive free radicals, thereby enhancing the efficiency of contaminants degradation and bacterial disinfection.

Photocatalytic Degradation of BPA

To demonstrate the physicochemical properties of the samples discussed, the effect of the N-doping concentration on the photocatalytic degradation of BPA was investigated. As shown in Fig. 6(a) and 6(b), the photolysis experiment reveals that BPA is stable and resistant to degradation under simulated solar light alone. The pure TiO_2 sample exhibits the weakest photocatalytic activity, degrading only 46.43% of BPA after 4 h of irradiation, with a degradation rate constant of 0.19×10^{-2} min^{-1} (Fig. 6(b)). In comparison, the TS5 sample achieves 80.31% BPA removal efficiency from aqueous solution after the same period, significantly higher than that of the pristine TiO_2. Notably, nitrogen doping further enhances photocatalytic activity. The TS5N10 sample shows the highest performance, degrading 83.90% BPA after 4 h of irradiation. As depicted in Fig. 6(c), only about 17.1% of BPA removal over TS5N10 occurs during the initial 60-min adsorption process, with equilibrium adsorption established within 30 min.

Furthermore, photocatalytic removal accounts for 66.8% (Fig. 6(d)). This observation demonstrates that the total BPA removal is primarily driven by the photocatalytic process. The kinetic curves of BP A degradation for all the photocatalysts follow the pseudo-first-order kinetic model with the $R^2 > 0.96$. The

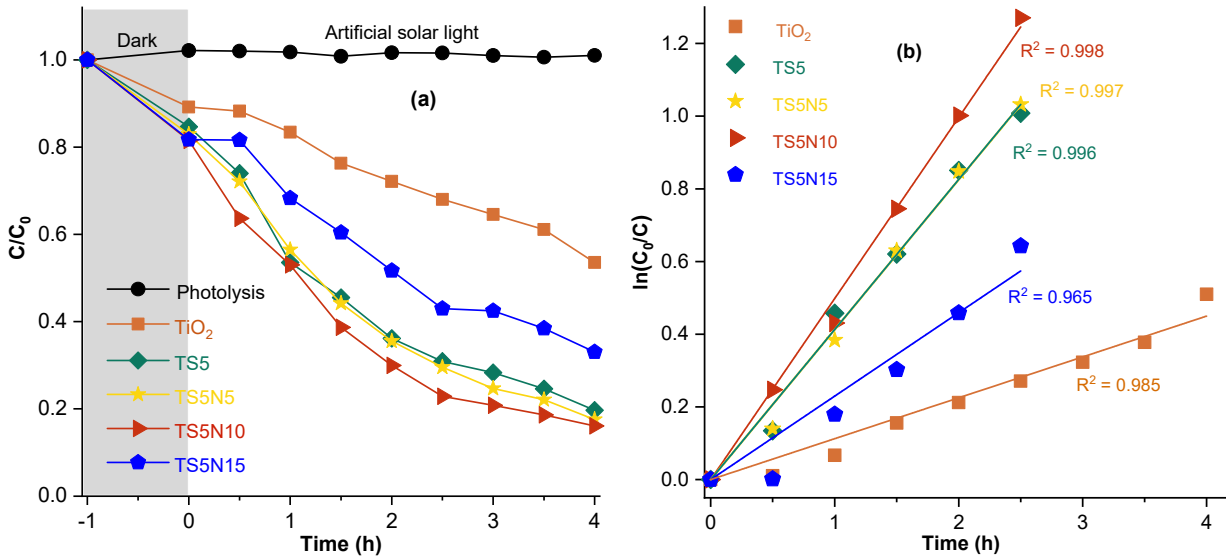

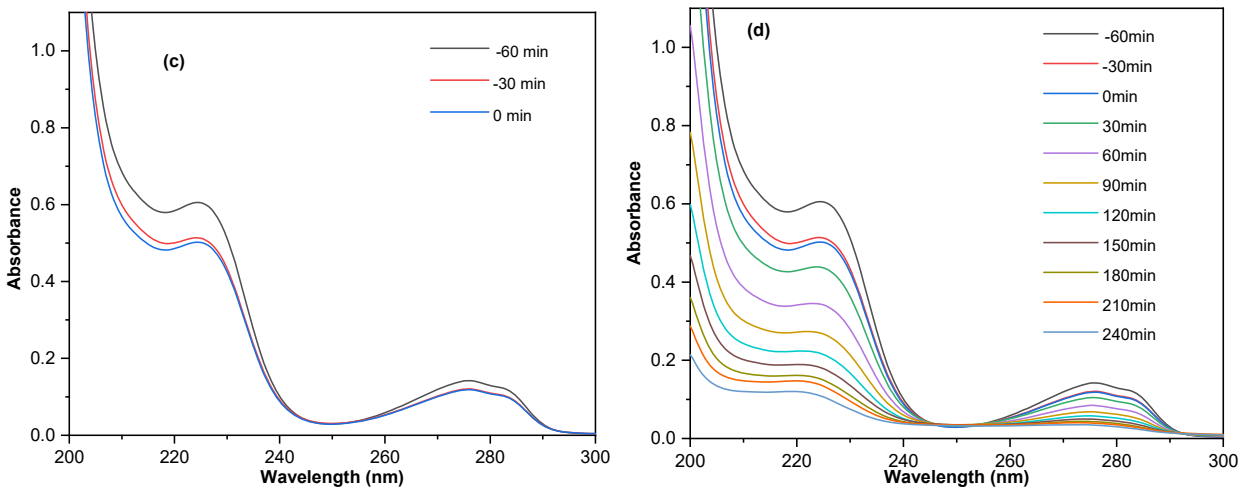

Fig 6. (a) Photocatalytic degradation curves and (b) pseudo-first-order rate constants of BPA degradation under simulated solar light irradiation; UV-vis absorption spectra of (c) adsorption and (d) degradation process of BPA over the TS5N10 catalyst

degradation rate constant for TS5N10 is calculated to be 0.83×10^{-2} min^{-1}, which is 4.4 times higher than that of pristine TiO_2 and 1.2 times higher than that of TS5. The improvement of photocatalytic activity of N-doped TS5 composites consistent with the results of XRD, BET, DRS, and PL, which the substitution of N elements alters the intrinsic properties of TiO_2-SiO_2 structure, improves the light absorption and inhibits the e^-/h^+ recombination rate. However, the BPA degradation efficiency decreases to 66.98% by using TS5N15. The excessive N contents (15%) can lead to the trapping of photogenerated electrons during transport process, thereby reducing the photocatalytic activity toward BPA degradation [39]. Consequently, TS5N10 composite with an appropriate N concentration was chosen as the material with superior photocatalytic activity.

To exploit the role of different reactive species in the photocatalytic process, trapping experiments were performed by introducing scavenger agents into the reaction system. As shown in Fig. 7, the BPA degradation efficiency slightly decreases to 78.1 and 76.5% in the presence of IPA and BQ, respectively. This observation reveals that •OH and superoxide $•O^{2-}$ are not the primary species involved in the photocatalytic process. In contrast, the BPA removal yield drops drastically to 18.2% upon the addition of EDTA-2Na, emphasizing the critical role of photogenerated holes (h^+) in the photocatalytic system.

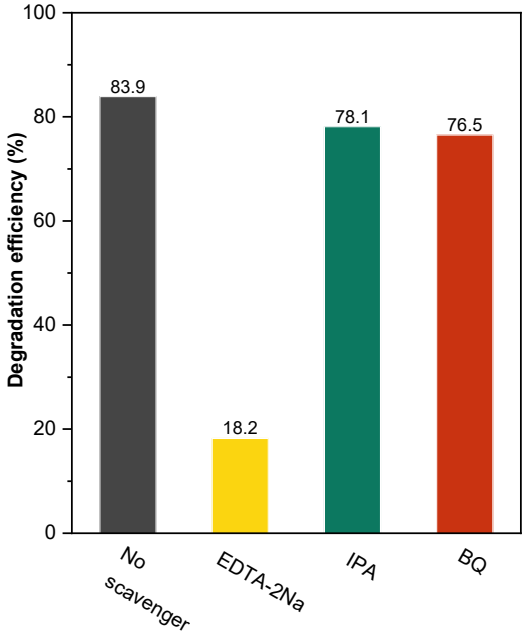

Fig 7. The trapping experiments for degradation of Bisphenol A over TS5N10 photocatalyst

Photocatalytic Disinfection of *E. coli*

The enhanced photocatalytic activity of N-doped TS5 was further validated through its disinfection effectiveness against *E. coli*. As shown in Fig. 8, the control sample, which lacked both light irradiation and photocatalyst, demonstrated normal *E. coli* survival. Additionally, a photolysis experiment was conducted to assess the direct impact of the utilized light source on

bacterial survival. The result shows that *E. coli* still maintained its cell density after 3 h of illumination, confirming the negligible effect of utilized light source alone. In contrast, all photocatalysts combined with light irradiation exhibited significant disinfection capabilities, with complete inactivation of *E. coli* cells observed after 3 h of irradiation. Remarkably, the TS5N10 sample achieved complete disinfection of *E. coli* within just 1.5 h of irradiation, outperforming the other samples, which required over 2 h to achieve similar result. This superior performance highlights the efficacy of TS5N10 in rapid bacterial disinfection under solar-like light conditions.

To further support these findings, visual images of *E. coli* colony over irradiation time versus different catalysts are presented in Fig. 9. Initially, the *E. coli* cell density on all three LB plates is around $D = 10^3$. After 1.5 h exposing to light source, the bacterial community density is significantly different. The colonies completely disappear on TS5N10 composite, while TiO_2 and TS5 showed little decrease of cell survival. The colonies finally observe on only TS5 sample after 2 h of irradiation, showing the better photoactivity of TiO_2 in comparison with TS5. This result aligns with that of the BPA photocatalytic

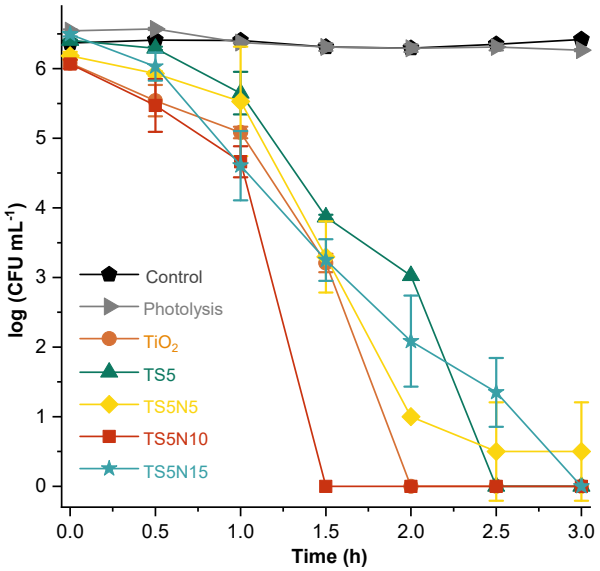

Fig 8. Antibacterial activity of TiO_2, TS5 and N-doped TS5 photocatalysts

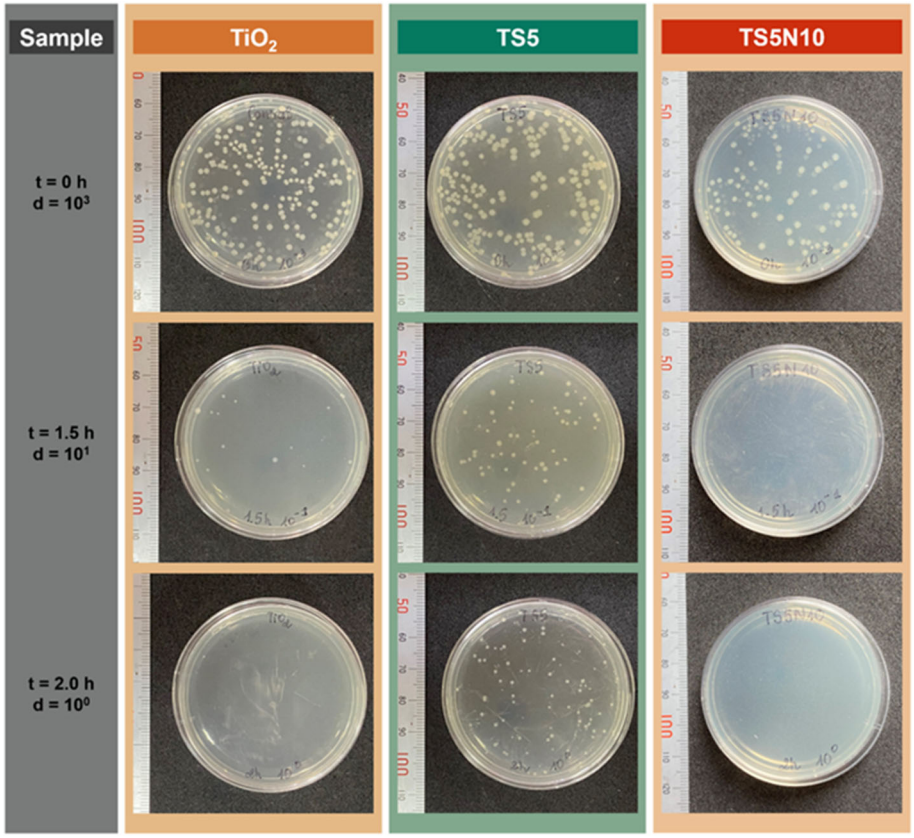

Fig 9. Visual images of colony forming units on the LB agar plates at the time t = 0, 1.5, and 2 h over samples

degradation, which proved TS5N10 has the strongest photocatalytic activity.

Simultaneous Photocatalytic Degradation of BPA and Disinfection of *E. coli*

To further evaluate the photocatalytic efficiency of TS5N10 in a dual-contaminant system, simultaneous degradation of BPA and disinfection of *E. coli* were conducted (as presented in Fig. 10) under identical conditions to the individual tests (Fig. 10(a)). The results, illustrated in Fig. 10(b), reveal a slight decline in photocatalytic performance when both contaminants are present simultaneously. Specifically, the degradation efficiency of BPA in mixture is approximately 10% lower than in the individual system (Fig. 10(a)). This reduction can be attributed to the competitive adsorption on the active sites of the catalyst surface by BPA molecules and *E. coli* cells, which limits the availability of these sites for photocatalytic reactions. Similarly, the disinfection efficiency in the dual-contaminant system is slower compared to the individual disinfection system. Complete inactivation of *E. coli* requires up to 3 h of in the simultaneous process, whereas it only took 1 h in the single-contaminant case. These observations align with prior studies [29,40], which suggest complex interactions between degradation and disinfection processes during photocatalytic treatments, potentially leading to competition for reactive species and surface sites. Despite these challenges, TS5N10 demonstrates robust performance in handling mixed contaminant systems.

■ CONCLUSION

In summary, solar-light-driven N-doped TiO_2-SiO_2 photocatalysts were successfully synthesized through a straightforward sol-gel method. The incorporation of nitrogen atoms into TiO_2-SiO_2 structure not only enhanced the visible light absorption by narrowing the bandgap of TiO_2-SiO_2 but also improved charge separation and inhibited recombination. Among the synthesized materials, the TS5N10 composite manifests exceptional photocatalytic activity, significantly outperforming other samples in both degrading BPA and inactivating *E. coli*. Under separate photocatalytic processes, TS5N10 achieved up to 83.9% BPA degradation after 4 h of irradiation, while *E. coli* cells were completely inactivated within 1.5 h of irradiation. Photo-generated holes were identified as the primary active species responsible for the photodegradation. Although the simultaneous treatment of BPA and *E. coli* resulted in reduced efficiency for both BPA degradation and bacterial inactivation compared to individual treatments, the TS5N10 demonstrated robust performance in handling complex contaminants systems. These findings underscore the potential of TS5N10 for

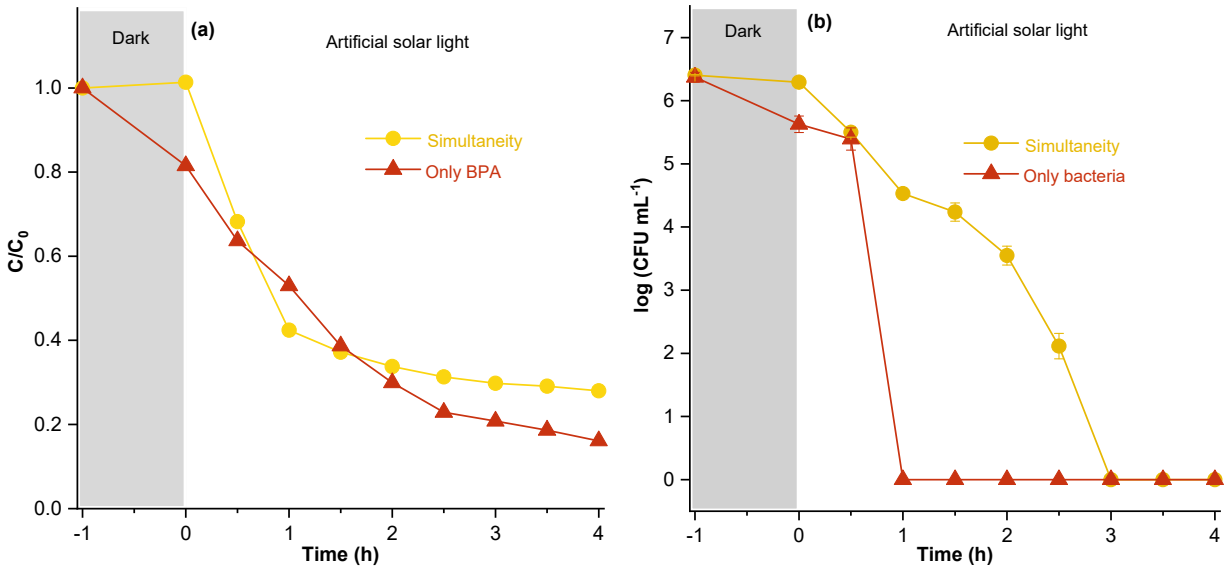

Fig 10. Simultaneous treatment of (a) BPA and (b) *E. coli* over TS5N10 photocatalyst

addressing multifaceted challenges in wastewater treatment. Further research is needed to optimize its catalytic performance for practical applications.

■ ACKNOWLEDGMENTS

We acknowledge Ho Chi Minh City University of Technology (HCMUT), VNU-HCM for supporting this study.

■ CONFLICT OF INTEREST

The authors have no conflict of interest to declare.

■ AUTHOR CONTRIBUTIONS

Minh Vien Le: Conceptualization, Formal analysis, Investigation, Methodology, Visualization, Writing-Original Draft, Writing-Review & Editing. Trung Tan Tran: Visualization, Writing-Review & Editing. Anh Hoang Hoang: Conceptualization, Methodology, Supervision. Hien Thao Nguyen: Formal analysis, Investigation, Methodology, Vu Truong-Son Le: Formal analysis, Methodology, Van Hoang Luan: Conceptualization, Writing-Review & Editing. Manh Thang Ngo: Visualization, Writing-Review & Editing. All authors agreed to the final version of this manuscript.

■ REFERENCES

[1] Khatri, N., and Tyagi, S., 2015, Influences of natural and anthropogenic factors on surface and groundwater quality in rural and urban areas, *Front. Life Sci.*, 8 (1), 23–39.

[2] Salehi, M., 2022, Global water shortage and potable water safety; Today's concern and tomorrow's crisis, *Environ. Int.*, 158, 106936.

[3] Orge, C.A., Faria, J.L., and Pereira, M.F.R., 2017, Photocatalytic ozonation of aniline with TiO_2-carbon composite materials, *J. Environ. Manage.*, 195, 208–215.

[4] Lu, Q., Li, N., and Zhang, X., 2022, Supramolecular recognition PVDF/PVA ultrafiltration membrane for rapid removing aromatic compounds from water, *Chem. Eng. J.*, 436, 132889.

[5] Sambaza, S.S., Maity, A., and Pillay, K., 2020, Polyaniline-coated TiO_2 nanorods for photocatalytic degradation of bisphenol A in water, *ACS Omega*, 5 (46), 29642–29656.

[6] Stec, J., Kosikowska, U., Mendrycka, M., Stępień-Pyśniak, D., Niedźwiedzka-Rystwej, P., Bębnowska, D., Hrynkiewicz, R., Ziętara-Wysocka, J., and Grywalska, E., 2022, Opportunistic pathogens of recreational waters with emphasis on antimicrobial resistance—A possible subject of human health concern, *Int. J. Environ. Res. Public Health*, 19 (12), 7308.

[7] Bhandari, H., Garg, S., and Gaba, R., 2021, Advanced nanocomposites for removal of heavy metals from wastewater, *Macromol. Symp.*, 397 (1), 2000337.

[8] Morones-Esquivel, M.M., Núñez-Núñez, C.M., Hernández-Mendoza, J.L., and Proal-Nájera, J.B., 2022, Bacterial communities in effluents rich in phenol and their potential in bioremediation: Kinetic modeling, *Int. J. Environ. Res. Public Health*, 19 (21), 14222.

[9] Le, P.N.M., Tran, H.T., Ngo, T.H., Truong, V.T., and Le, M.V., 2024, The role of iron dopant on the photocatalytic performance of anatase TiO_2: Synthesis, characterization, and removal of bisphenol-A under simulated natural light, *J. Appl. Sci. Eng.*, 27 (6), 2675–2685.

[10] Rojviroon, T., and Sirivithayapakorn, S., 2018, *E. coli* bacteriostatic action using TiO_2 photocatalytic reactions, *Int. J. Photoenergy*, 2018 (1), 8474017.

[11] Long, M., Wang, J., Zhuang, H., Zhang, Y., Wu, H., and Zhang, J., 2014, Performance and mechanism of standard nano-TiO_2 (P-25) in photocatalytic disinfection of foodborne microorganisms–*Salmonella typhimurium* and *Listeria monocytogenes*, *Food Control*, 39, 68–74.

[12] Pantaroto, H.N., Ricomini-Filho, A.P., Bertolini, M.M., Dias da Silva, J.H., Azevedo Neto, N.F., Sukotjo, C., Rangel, E.C., and Barão, V.A., 2018, Antibacterial photocatalytic activity of different crystalline TiO_2 phases in oral multispecies biofilm, *Dent. Mater.*, 34 (7), e182–e195.

[13] Huang, J., Dou, L., Li, J., Zhong, J., Li, M., and Wang, T., 2021, Excellent visible light responsive photocatalytic behavior of N-doped TiO_2 toward decontamination of organic pollutants, *J. Hazard. Mater.*, 403, 123857.

[14] Mahanta, U., Khandelwal, M., and Deshpande, A.S., 2022, TiO_2@SiO_2 nanoparticles for methylene blue removal and photocatalytic degradation under natural sunlight and low-power UV light, *Appl. Surf. Sci.*, 576, 151745.

[15] Murcia, J.J., Ávila-Martínez, E.G., Rojas, H., Navío, J.A., and Hidalgo, M.C., 2017, Study of the *E. coli* elimination from urban wastewater over photocatalysts based on metallized TiO_2, *Appl. Catal., B*, 200, 469–476.

[16] Cani, D., van der Waal, J.C., and Pescarmona, P.P., 2021, Highly-accessible, doped TiO_2 nanoparticles embedded at the surface of SiO_2 as photocatalysts for the degradation of pollutants under visible and UV radiation, *Appl. Catal., A*, 621, 118179.

[17] Zhang, L., Guo, J., Hao, B., and Ma, H., 2022, WO_3/TiO_2 heterojunction photocatalyst prepared by reactive magnetron sputtering for Rhodamine B dye degradation, *Opt. Mater.*, 133, 113035.

[18] Chen, X., and Burda, C., 2008, The electronic origin of the visible-light absorption properties of C-, N- and S-doped TiO_2 nanomaterials, *J. Am. Chem. Soc.*, 130 (15), 5018–5019.

[19] Yu, H., Zhang, M., Wang, Y., Lv, J., Liu, Y., He, G., and Sun, Z., 2021, Low-temperature strategy for vapor phase hydrothermal synthesis of C\N\S-doped TiO_2 nanorod arrays with enhanced photoelectrochemical and photocatalytic activity, *J. Ind. Eng. Chem.*, 98, 130–139.

[20] Le, T.T.T., Tran, D.T., and Danh, T.H., 2021, Remarkable enhancement of visible light driven photocatalytic performance of TiO_2 by simultaneously doping with C, N, and S, *Chem. Phys.*, 545, 111144.

[21] Dey, K., Vaidya, S., Gobetti, A., Ramorino, G., and Ganguli, A.K., 2022, Facile synthesis of N-doped biphasic TiO_2 nanoparticles with enhanced visible light-driven photocatalytic performance, *Mater. Today Commun.*, 33, 104690.

[22] Nguyen, D.T., Ho, T.N.S., and Le, M.V., 2019, Removal of β-naphthol in water via photocatalytic degradation over N-TiO_2/SiO_2 nanocomposite under simulated solar light irradiation, *Chem. Eng. Trans.*, 72, 1–6.

[23] Jesus, M.A.M.L., Ferreira, A.M., Lima, L.F.S., Batista, G.F., Mambrini, R.V., and Mohallem, N.D.S., 2021, Micro-mesoporous TiO_2/SiO_2 nanocomposites: Sol-gel synthesis, characterization, and enhanced photodegradation of quinoline, *Ceram. Int.*, 47 (17), 23844–23850.

[24] Esfandiari, N., Kashefi, M., Mirjalili, M., and Afsharnezhad, S., 2021, On the adsorption kinetics and mechanism of enhanced photocatalytic activity of Fe_3O_4-SiO_2-TiO_2 core-multishell nanoparticles against *E. coli*, *J. Biomed. Mater. Res., Part A*, 109 (2), 181–192.

[25] Yuwendi, Y., Ibadurrohman, M., Setiadi, S., and Slamet, S., 2022, Photocatalytic degradation of polyethylene microplastics and disinfection of *E. coli* in water over Fe-and Ag-modified TiO_2 nanotubes, *Bull. Chem. React. Eng. Catal.*, 17 (2), 263–277.

[26] Nguyen, T.V., Le, P.N.M., Huynh, N.D.T., Ngo, T.H., Huynh, H.T., and Le, M.V., 2022, The synergistic effect of N-doped TiO_2-SiO_2 nanocatalysts and peroxydisulfate towards improving Bisphenol A photodegradation efficiency, *MNIJ*, 2 (1), 1–14.

[27] Le, M.V., Tai, H.H., Oanh, N.T.K., Thang, N.M., and Suong, H.T.N., 2020, Enhanced photocatalytic degradation performance of bisphenol A over TiO_2-SiO_2 photocatalyst by improving specific surface area under simulation natural light, *Vietnam J. Catal. Adsorpt.*, 9 (4), 49–57.

[28] Abbasi_Asl, H., Sabzehmeidani, M.M., Ghaedi, M., and Moradi, Z., 2023, Bifunctional quaternary magnetic composite as efficient heterojunctions photocatalyst for simultaneous photocatalytic visible light degradation of dye and herbicide pollutants from water and bacterial disinfection, *J. Environ. Manage.*, 345, 118656.

[29] He, J., Zeng, X., Lan, S., and Lo, I.M., 2019, Reusable magnetic Ag/Fe, N-TiO_2/Fe_3O_4@SiO_2 composite for simultaneous photocatalytic disinfection of *E. coli* and degradation of bisphenol A in sewage under visible light, *Chemosphere*, 217, 869–878.

[30] Vo, N.Q.D., Huynh, N.D.T., Le, M.V., Vo, K.D., and Vo, D.V.N., 2020, Fabrication of Ag-photodeposited

TiO_2/cordierite honeycomb monolith photoreactors for 2-naphthol degradation, *J. Chem. Technol. Biotechnol.*, 95 (10), 2628–2637.

[31] Tamer, T.M., Hassan, M.A., Omer, A.M., Baset, W.M.A., Hassan, M.E., El-Shafeey, M.E.A., and Eldin, M.S.M., 2016, Synthesis, characterization and antimicrobial evaluation of two aromatic chitosan Schiff base derivatives, *Process Biochem.*, 51 (10), 1721–1730.

[32] Ren, C., Qiu, W., Zhang, H., He, Z., and Chen, Y., 2015, Degradation of benzene on $TiO_2/SiO_2/Bi_2O_3$ photocatalysts under UV and visible light, *J. Mol. Catal. A: Chem.*, 398, 215–222.

[33] Shifu, C., and Gengyu, C., 2006, The effect of different preparation conditions on the photocatalytic activity of TiO_2·SiO_2/beads, *Surf. Coat. Technol.*, 200 (11), 3637–3643.

[34] Dong, F., Zhao, W., Wu, Z., and Guo, S., 2009, Band structure and visible light photocatalytic activity of multi-type nitrogen doped TiO_2 nanoparticles prepared by thermal decomposition, *J. Hazard. Mater.*, 162 (2-3), 763–770.

[35] Kamani, H., Ashrafi, S.D., Lima, E.C., Panahi, A.H., Nezhad, M.G., and Abdipour, H., 2023, Synthesis of N-doped TiO_2 nanoparticle and its application for disinfection of a treatment plant effluent from hospital wastewater, *Desalin. Water Treat.*, 289, 155–162.

[36] Marques, J., Gomes, T.D., Forte, M.A., Silva, R.F., and Tavares, C.J., 2019, A new route for the synthesis of highly-active N-doped TiO_2 nanoparticles for visible light photocatalysis using urea as nitrogen precursor, *Catal. Today*, 326, 36–45.

[37] Cong, Y., Zhang, J., Chen, F., and Anpo, M., 2007, Synthesis and characterization of nitrogen-doped TiO_2 nanophotocatalyst with high visible light activity, *J. Phys. Chem. C*, 111 (19), 6976–6982.

[38] Le, P.H., Hieu, L.T., Lam, T.N., Hang, N.T.N., Truong, N.V., Tuyen, L.T.C., Phong, P.T., and Leu, J., 2018, Enhanced photocatalytic performance of nitrogen-doped TiO_2 nanotube arrays using a simple annealing process, *Micromachines*, 9 (12), 618.

[39] Wu, C., Dong, X., Wang, L., Zhang, L., and Liu, X., 2022, Preparation of N-TiO_2/SiO_2 composites by solvothermal method and their photocatalytic properties, *Mater. Res. Express*, 9 (5), 055002.

[40] He, H., Sun, S., Gao, J., Huang, B., Zhao, T., Deng, H., Wang, X., and Pan, X., 2020, Photoelectrocatalytic simultaneous removal of 17α-ethinylestradiol and *E. coli* using the anode of Ag and SnO_2-Sb 3D-loaded TiO_2 nanotube arrays, *J. Hazard. Mater.*, 398, 122805.